PNAS NEXUS

PNAS Nexus, 2025, 4, pgaf064

https://doi.org/10.1093/pnasnexus/pgaf064
Advance access publication 28 February 2025
Research Report

Direct observation of carbon dioxide adsorption and binding at the air/aqueous interface

Mokhtar Rashwan [a], Zhiwei Mao [b], Jacob S. Hirschi [b], Tim J. Zuehlsdorff [b], May Nyman [b,*] and Ahmet Uysal [a,*]

[a]Chemical Sciences and Engineering Division, Argonne National Laboratory, Lemont, IL 60439, USA
[b]Department of Chemistry, Oregon State University, Corvallis, OR 97331, USA
*To whom correspondence should be addressed: Email: ahmet@anl.gov (A.U.); Email: may.nyman@oregonstate.edu (M.N.)
Edited By Dennis Hartmann

Abstract

Carbon dioxide removal (CDR) involves reducing carbon dioxide (CO_2) concentrations. Developing new technologies and enhancing existing ones for extracting and converting CO_2 are ongoing areas of research. In all these technologies, the movement of CO_2 molecules through an interface is a common process. At liquid surfaces, the nanometer-thick interfacial region is expected to play a fundamental role in enhancing or hindering the process. The interface can have significantly different conditions, such as pH, ion concentration, and ion speciation, compared with the bulk. Despite this, our knowledge of the molecular-scale details of CO_2 capture and conversion at liquid interfaces is limited. Here, we report direct observation of CO_2 surface adsorption and conversion to bicarbonate at the air/aqueous interface of potassium orthovanadate solutions using vibrational sum frequency generation spectroscopy. We show that orthovanadate ions enhance the hydrated CO_2 population at the interface, indicated by a strong peak at 2,336 cm^{-1}. DFT calculations suggest that CO_2 molecules are bent with respect to their original linear structure, demonstrating the initiation of CO_2 to HCO_3^- conversion. With increasing orthovanadate concentration and/or time of exposure, the CO_2 peak disappears, and (bi)carbonate peaks appear. The characterization of the bulk solutions as well as the precipitated products suggests that the observed interfacial species are transient, different from the final products. This study provides a better understanding of CO_2 transport into aqueous media, not only for CDR technologies but also for environmental and atmospheric chemistry in general.

Keywords: carbon dioxide removal, interfaces, adsorption, sum frequency generation spectroscopy, peroxometalates

Significance Statement

Understanding the transport and reactivity of carbon dioxide (CO_2) at interfaces can significantly enhance CO_2 removal technologies. However, molecular-level investigations of CO_2 capture at liquid interfaces are scarce due to the complexity of these interfaces and the limited availability of surface-sensitive techniques. We present direct evidence of CO_2 adsorption and its conversion into (bi)carbonate products at the air/liquid interface, using vibrational sum frequency generation spectroscopy. This molecular-scale study lays the foundation for a predictive understanding of interfacial reaction conditions, which could be optimized for enhanced and continuous reactivity.

Introduction

Developing new carbon dioxide removal (CDR) technologies is an active area of research (1, 2). Carbon dioxide (CO_2) is selectively extracted from the atmosphere via different approaches, such as membranes, sorbents, and electrochemical and thermal swing (1, 3, 4). Some common sorbents include alkali/alkaline earth (hydr)oxides, mineral oxides, metal organic frameworks, and amine-based sorbents. Liquid sorbents are especially important as they are scalable and compatible with most industrial processes. The interfacial reactions during CO_2 capture and conversion are keys to the success of liquid sorbents. The nanometer-thick region at the liquid interface has significantly different properties, including different ion concentrations and ion-pairing behavior, pH gradients, and hydrophobic self-assembly (5, 6). Therefore, interfacial behavior cannot simply be deduced from bulk properties. Understanding the fundamental physical and chemical processes at these interfaces is crucial to develop and improve CDR technologies.

The interfacial behavior of carbonate, bicarbonate, and other related carbon capture products has been studied and debated extensively. Surface-sensitive sum frequency generation (SFG) spectroscopy studies of carbonate and bicarbonate solutions inferred the ion behavior via secondary effects on the interfacial water (7). Ambient pressure X-ray photoelectron spectroscopy and resonantly enhanced deep-UV second harmonic generation spectroscopy studies showed that carbonate anions are more

Competing Interest: The authors declare no competing interests.
Received: December 3, 2024. **Accepted:** February 12, 2025

abundant than the bicarbonate ions at the interface, in contrast to the widely used models, which suggest that doubly charged anions would be repelled from the interface due to the image charge interactions (8, 9).

Interfacial structure during CO_2 capture and conversion has been less explored. Combined X-ray reflectivity and neutron reflectivity studies investigated liquid/air interface during CO_2 capture in ionic liquid-propanol solutions and suggested that CO_2 is adsorbed with anions beneath the cation-rich top surface (10). Richmond and coworkers used SFG spectroscopy to study the reaction of highly concentrated monoethanolamine (MEA) solution and CO_2 at the air/liquid interface. They observed significant spectral differences at the air/MEA interface upon reaction with CO_2 (11, 12). Broadening of the methylene bending and stretching modes of MEA was observed, indicative of the presence of charged species at the interface, driving reorientation of the MEA and surface-active moieties. More importantly, the loss of the N–H bending mode and the presence of the amide II band (N–H deformation) upon reaction with CO_2 were signatures of the formation of amide-containing species (carbamic acid) upon the reaction with CO_2 (11–13). Premadasa et al. used SFG spectroscopy and MD simulations to study the CO_2 capture at the air/aqueous amino acid interface (leucine, valine, and phenylalanine) under highly alkaline conditions (pH 12), at which the anionic species predominate (14). The spectral variations of the CH stretches were used as molecular reporters on the structural and orientational changes promoted by CO_2 capture. In a recent study, the same team demonstrated that added bicarbonate, a possible direct air capture (DAC) product concentrated in the subsurface region, induced concentration and charge gradients at the interface (6). Neither CO_2 nor (bi)carbonate species were directly observed at the air/liquid interface in these studies.

Recently, we reported the direct observation of (bi)carbonate species at the air/liquid interface of niobium polyoxometalate aqueous solutions under enhanced CO_2 atmosphere. SFG studies showed a vibrational signature of bidentate bicarbonate (1,412 cm^{-1}) upon exposure to CO_2, whose intensity was countercation dependent (15). No interfacial signature of hydrated CO_2 was observed in that study.

Here, we provide a direct observation of the adsorption and binding of CO_2 and the subsequent formation of (bi)carbonate species at the air/liquid interface of orthovanadate solutions using SFG spectroscopy. Prior, inorganic oxoanions were shown to enhance the hydration and absorption of CO_2 into aqueous solutions (16–18). Among all the studied oxoanions, orthovanadate has the highest catalytic efficiency for CO_2 hydration, providing the ideal conditions to observe interfacial CO_2 (17, 18).

Solutions for SFG measurements were prepared by dissolving orthovanadate and orthomolybdate salts in deionized water. Solutions in a small Teflon dish were placed inside a custom-made, sealed chamber for controlled atmosphere (Fig. 1a). Multiple spectral regions were scanned for signatures of carbonate and CO_2, in addition to the OH region of water (2,800–3,800 cm^{-1}). In a typical SFG measurement, a fixed visible (532 nm) and tunable infrared (IR) (1,000–4,000 cm^{-1}) picosecond pulsed lasers is overlapped spatially and temporally at the air/liquid interface. The generation of a nonlinear SFG signal is forbidden in the centrosymmetric medium and therefore can only be generated at the interface where the symmetry is broken. The SFG signal is proportional to the square of the second-order nonlinear susceptibility ($\chi^{(2)}$) (see Materials and methods). Therefore, the SFG signal intensity is related to both number density and the orientational ordering of the oscillators. All SFG data were normalized against nonresonant SFG signal collected from a gold surface to correct for the variations in the laser power and IR absorption due to the atmospheric CO_2. Bulk solution conditions were investigated by Fourier transform IR spectroscopy (FTIR) measurements. The final products were characterized by FTIR, powder X-ray diffraction (PXRD), and thermogravimetric analysis–mass spectrometry (TGA–MS).

Results

Direct observation of interfacial CO_2

Figure 1b shows the SFG spectra collected at the air/100 mM aqueous K_3VO_4 interface in the absence and presence of excess CO_2 from 2,200 to 2,400 cm^{-1}. In the presence of ambient CO_2, the orthovanadate SFG spectrum shows two spectral dips at 2,340 and 2,360 cm^{-1} (Fig. S1). The peak positions of these two features are consistent with previously reported CO_2(g) features at 2,336 and 2,362 cm^{-1} as the R branch and P branch of CO_2(g) rotational–vibrational spectrum (19, 20). Upon introducing CO_2 into the sample cell, the CO_2(g) R branch and P branch disappear and a narrow, sharp peak at 2,336 cm^{-1} grows (Fig. 1b, red spectrum). We assign this peak to the υ_3 asymmetric stretch of CO_2, which is at 2,350 cm^{-1} in vacuum (19). The emergence of this peak is a direct indication of CO_2 hydration and adsorption at the air/water interface in CO_2-saturated atmosphere (19, 21). This is unexpected because CO_2 is a centrosymmetric molecule, and therefore, it cannot have a vibrational mode that is both Raman and IR active (a necessary condition for a vibrational mode to be SFG active). We investigated the validity and the implications of this observation in depth.

We first investigate the kinetics and the stability of CO_2 adsorption. When 100 mM orthovanadate solution is exposed to a 40-mmol/dm^3 CO_2 atmosphere (pCO_2 ~1 atm), the peak is observed as early as 10 min, and its intensity increases for 60 min and reaches a plateau (Fig. 1d, inset). After 60 min, we removed the lid of the sample cell completely, exposing it to the ambient atmosphere. The peak intensity dropped very slowly to 80% of its maximum within 60 min, indicative of a long-lived population, possibly kinetically trapped in this metastable state. We also simultaneously probed the spectral regions for any CO_2 capture products, such as carbonates and bicarbonates, but did not see any peaks within the first 2 h.

Figure 2a–c shows the increase of the surface-adsorbed CO_2 with the increasing concentration of CO_2 in the sample chamber. Each data point is measured with a fresh solution (100 mM VO_4^{3-}) with variable CO_2 atmospheric concentration for 30 min. Assuming that the overall orientational ordering of the interfacial CO_2 is similar for all concentrations, we can calculate the relative coverage of the adsorbed CO_2 from the amplitude of the SFG signal. Then, it is possible to fit the adsorption isotherm by the Langmuir model:

$$q_e = \frac{q_{max} K_L C_e}{1 + K_L C_e} \quad (1)$$

where q_e, q_{max}, K_L, and C_e represent the adsorbed CO_2 amount (mmol/dm^2), maximum CO_2 capacity (mmol/dm^2), Langmuir constant (dm^3/mmol), and CO_2 equilibrium concentration (mmol/dm^3), respectively.

Fitting the experimental data (SFG amplitude) to Eq. 1 shows a good agreement with the Langmuir adsorption isotherm (Fig. 2b). Plotting the SFG amplitude to the linearized Langmuir equation

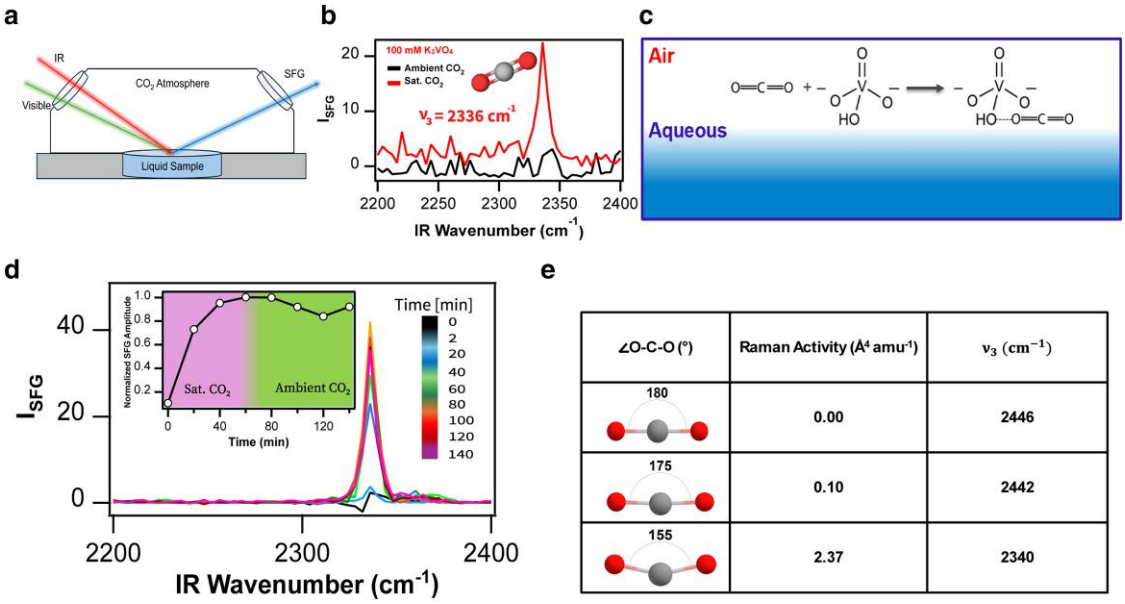

Fig. 1. a) Scheme of SFG experimental setup, SFG measurements were performed at the air/liquid interface in 1.0-inch diameter Teflon dish placed inside a tightly sealed chamber with two KBr windows for the input and output laser beams. b) *ssp*-SFG spectra collected at the air/100 mM aqueous K_3VO_4 interface with (red) and without (black) excess CO_2 from 2,200 to 2,400 cm^{-1}. The 2,336 cm^{-1} peak observed upon CO_2 infusion is assigned to the CO_2 asymmetric stretching mode, indicating adsorption of CO_2 at the air/liquid interface. c) Schematic of CO_2 adsorption at the air/liquid interface, showing the direct interaction of the hydroxyl group of protonated orthovanadate with CO_2. d) Time-dependent *ssp*-SFG spectra collected at the air/100 mM aqueous K_3VO_4 interface before and after excess CO_2 are introduced at t = 0 from 2,200 to 2,400 cm^{-1}. d) Inset: Amplitude of the 2,336 cm^{-1} peak normalized to the maximum amplitude at 60 min of CO_2 exposure from spectra in (d). The SFG spectra (and amplitude) collected after CO_2 purging stopped (after 60 min) show that the CO_2 2,336 cm^{-1} peak persists, demonstrating an indicative of a long-lived population, possibly kinetically trapped in this metastable state. e) CO_2 bond angle, Raman activity, and υ_3 symmetric stretch peak frequency from DFT calculations, showing enhanced Raman activity with CO_2 bending, which can be achieved through molecular interactions with the orthovanadate anions.

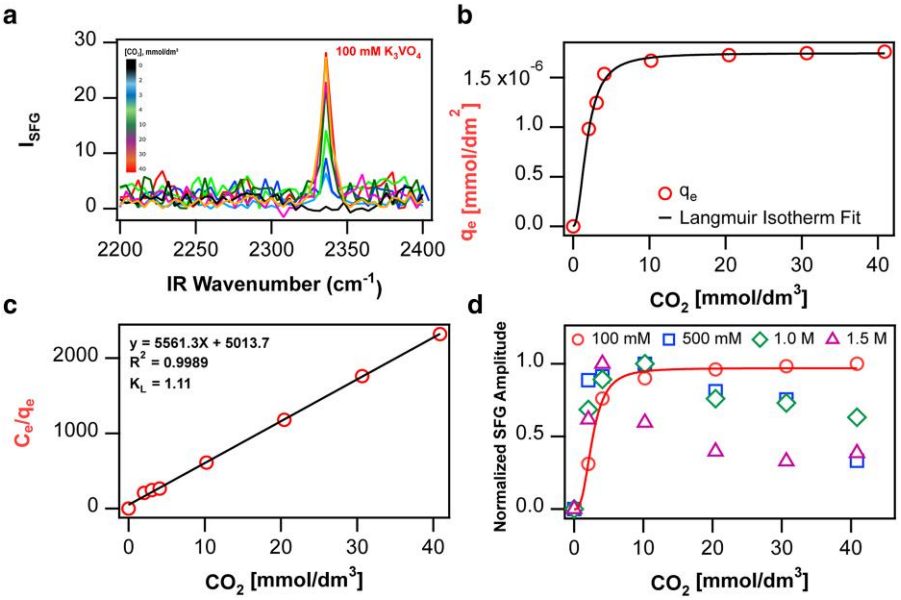

Fig. 2. a) CO_2 concentration-dependent *ssp*-SFG spectra collected at the air/aqueous 100 mM K_3VO_4 from 2,200 to 2,400 cm^{-1} collected after 30 min of reaction with CO_2. b) Adsorbed CO_2 concentration calculated from SFG amplitudes of (a) SFG spectra; black is the Langmuir isotherm fit. c) Linearized Langmuir isotherm fit line, with $R^2 = 0.9989$ and Langmuir constant of 1.11 dm^3/mmol. d) Comparison of the amplitude of the 2,336 cm^{-1} peak normalized to the maximum amplitude for each individual VO_4^{3-} concentration, collected after 30 min of reaction with CO_2 for 100 mM, 500 mM, 1.0 M, and 1.5 M K_3VO_4 solutions.

(Eq. 2) yielded a straight line with a correlation coefficient, R^2 of 0.9989 and a Langmuir constant 0.080 dm^3/mmol (Fig. 2c).

$$\frac{C_e}{q_e} = \frac{C_e}{q_{max}} + \frac{1}{q_{max}\, K_L} \qquad (2)$$

Given that vanadium speciation is highly dependent on vanadium concentration, which would ultimately control its catalytic activity for CO_2 hydration, we also conducted SFG measurements with varying orthovanadate concentrations. Figure 2d shows the amplitude of the CO_2 asymmetric stretch normalized to the maximum

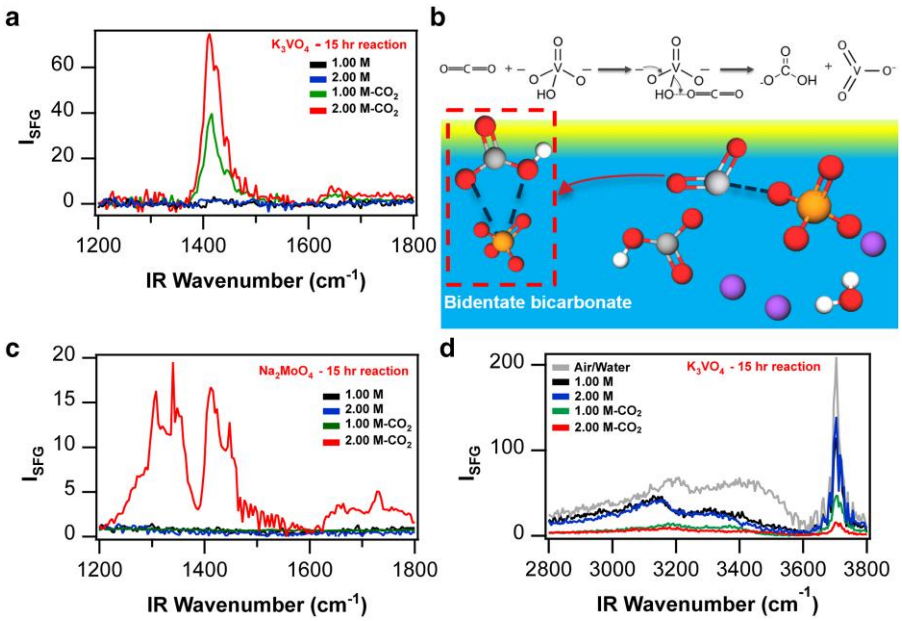

Fig. 3. a) *ssp*-SFG spectra collected at the air/aqueous interface of 1.0 and 2.0 M K_3VO_4 solutions before and after reaction with CO_2 for ~15 h from 1,200 to 1,800 cm^{-1}. b) Schematic showing the formation of bidentate bicarbonate at the interface after 15 h of exposure to CO_2. The written mechanism shows that the protonated orthovanadate anion binds directly to CO_2 via a carbonic anhydrase mechanism, followed by the formation of bicarbonate and metavanadate species (orthovanadate speciation is explained in the Discussion section and shown in Fig. S9). c) *ssp*-SFG spectra collected at the air/water interface of 1.0 and 2.0 M aqueous Na_2MoO_4 solutions before and after reaction with CO_2 for ~15 h from 1,200 to 1,800 cm^{-1}. After reaction of K_3VO_4 with CO_2, ~1,412 and 1,640 cm^{-1} peaks, assigned to the symmetric and asymmetric stretching modes of bidentate bicarbonate species, are observed. After reaction of 2 M Na_2MoO_4 with CO_2, multiple SFG features were observed at 1,308, 1,340, 1,412, 1,448, 1,640, and 1,728 cm^{-1}, assigned to stretches of differently coordinated (bi)carbonate species. d) *ssp*-SFG spectra collected at the air/liquid interface of 1 and 2 M K_3VO_4 solutions before and after reaction with CO_2 between 2,800 and 3,800 cm^{-1}. The neat air/water spectrum is shown for comparison.

SFG amplitude for SFG spectra collected at different vanadium concentrations (500 mM, 1 M, and 1.5 M) while increasing CO_2 concentration. CO_2 adsorption was found to increase with CO_2 concentration and saturate only at 100 mM orthovanadate. At higher vanadium concentrations, CO_2 hydration at the interface increased at low CO_2 levels, then dropped thereafter, especially with higher orthovanadate concentrations. These results indicate that once the interfacial (bi)carbonate formation starts the hydrated CO_2 species can more easily transform, similar to a nucleation event. Indeed, we were not able to observe any interfacial CO_2 at 2 M bulk orthovanadate concentration, suggesting that at this concentration even the ambient CO_2 is enough to start (bi)carbonate formation in a few minutes.

Direct observation of interfacial carbon capture products

As we will discuss in detail below, these results suggest that we are observing a metastable transient species of orthovanadate–CO_2 at the interface. To observe the final carbonate products, we exposed our samples to a saturated CO_2 atmosphere for ~15 h and investigated the possible formation of interfacial (bi)carbonate species. SFG spectra collected after longer exposure of 1 and 2 M orthovanadate solutions to CO_2 show the growth of two new SFG features at ~1,412 and 1,640 cm^{-1} (Fig. 3a, green and red spectra). The CO_2 asymmetric stretch is not observed simultaneously with these two features. We attribute these two peaks to the symmetric and asymmetric stretching modes of bidentate bicarbonate formed by CO_2 binding, respectively (22–26). These spectra are very similar to the bicarbonate species we observed at the air/aqueous interface of $[Nb_6O_{19}]^{8-}$ solutions. Also, in an SFG study of carboxylic acid films at the air/liquid interface, Sthoer et al. (24) observed intensity increase of the 1,416 cm^{-1} COO^- symmetric stretch and a drop in the C=O stretch of arachidic acid with increasing Y^{3+} and La^{3+} ion concentrations due to the increased metal binding of the carboxylic acid monolayer. The presence of these two modes indicates CO_2 binding and conversion to (bi)carbonate upon reaction with orthovanadate (scheme in Fig. 3b). At 2 M, the bicarbonate SFG features are more intense and broader (Fig. 3a, red spectrum), suggesting increased carbonate formation and heterogeneity of the air/liquid interface at higher orthovanadate concentration. We only see the spectral signatures of CO_2 hydration and binding as bicarbonate in the *ssp* polarization combination, suggesting that the CO_2 molecules are parallel to the air/water interface (no spectral signatures were observed in *ppp* or *sps* polarization combinations).

To compare the carbon capture activity of the orthovanadate anion with other transition metal oxoanions, we also collected SFG spectra on the air/aqueous molybdate (Na_2MoO_4) interface of 1 and 2 M solutions after reaction with CO_2 for ~15 h (K_2MoO_4 did not dissolve completely at equivalent concentration as K_3VO_4, hence not used for comparison). No spectral evidence of adsorption of CO_2 or binding as carbonates was observed below 2 M. At 2 M, we see evidence of CO_2 capture and binding as (bi)carbonate species (Fig. 3c), indicated by multiple (bi)carbonate features (Table S1).

Interfacial water behavior

The formed (bi)carbonate species at the air/liquid interface affects the orientation and structure of interfacial water (Fig. 3d) (7, 13, 27). A typical air/water SFG spectrum consists of two different water populations: hydrogen-bonded and nonhydrogen-bonded OH populations. The hydrogen-bonded OH oscillators consist of three broad peaks, 3,100, 3,200, and 3,400 cm^{-1}, from strongly to weakly hydrogen-bonded OH groups, respectively. The

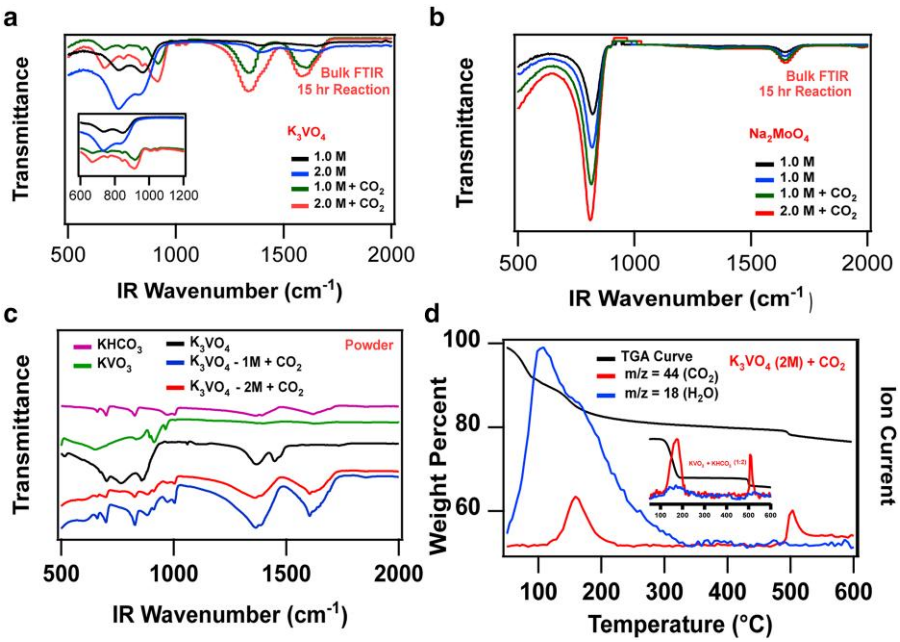

Fig. 4. a) Bulk ATR-FTIR spectra of K_3VO_4 before and after reaction with CO_2. Inset is a zoom on the 600–1,200 cm^{-1} region showing the appearance of two new peaks at 670 and 916 cm^{-1} due to the symmetric stretch of VO_2 and asymmetric stretch of VOV of the newly formed metavanadate species, in addition to the 1,010 and 1,045 cm^{-1} carbonate stretches. b) Bulk ATR-FTIR spectra of Na_2MoO_4 before and after reaction with CO_2. c) FTIR spectra of solid product of K_3VO_4 reaction with CO_2, spectra of pure $KHCO_3$ and KVO_3 are included for comparison. d) TGA–MS of the solid product from 2 M K_3VO_4 solution infused with CO_2, inset shows the TGA–MS of the mixture of $KHCO_3$ and KVO_3. The thermogravimetric signal is black. The red and blue traces are the signals of CO_2 and H_2O by MS.

nonhydrogen-bonded (free) OH groups, dangling out from the surface, vibrate at ~3,700 cm^{-1} (see gray spectrum in Fig. 3d) (28–30). SFG spectra collected at the air/aqueous orthovanadate interface are spectrally similar to the neat air/water spectrum, exhibiting three distinct features (Fig. 3d, black and blue spectra): two slightly red-shifted and less intense broad bands at 3,150 and 3,350 cm^{-1} due to strongly and weakly hydrogen-bonded water, and a dangling OH peak at ~3,700 cm^{-1}. The 2 M spectrum shows a weaker 3,150 band and a stronger free-OH peak compared with 1 M, highlighting the effect of the salt concentration on the hydrogen-bonding network at the air/water interface. Upon reaction with CO_2, the intensities of all the interfacial OH features significantly decrease (Fig. 3d, green and red spectra). The 3,350 cm^{-1} peak is barely observable at 2 M VO_4^{3-}. We attribute these significant spectral differences after reaction with CO_2 to the perturbation of the interfacial water populations by the newly formed (bi)carbonate/metavanadate species mentioned prior. The "merging" of hydrogen-bonded broad water band with the free-OH peak at 3,700 cm^{-1} is intriguing. At free air/water interface, these water populations have opposite orientations, creating a dip between their representative peaks, due to the destructive interference. The absence of this feature suggests that the hydrogen-bonded water population is also up-oriented like the free OH. This could be enhanced by the presence of anionic surface-active species.

Bulk carbon capture products

Bulk FTIR measurements were conducted on the same samples investigated by SFG. FTIR measurements revealed no noticeable spectral differences after short-time exposure of 100 mM potassium orthovanadate to CO_2 (Fig. S5). However, longer exposure to CO_2 gives rise to new (bi)carbonate and polynuclear metavanadate species (see Figs. 4a and S8), consistent with our proposed mechanism of CO_2 binding (Fig. 3b) (31, 32). In contrast, no new products were formed from the reaction of sodium orthomolybdate with CO_2 (Fig. 4b), suggesting that the formed surface/interface active (bi)carbonate species block the interface, hindering the migration of the formed species into the bulk. Characterization of the 2-day reaction solid product of 2 M orthovanadate solution using FTIR, TGA–MS, and PXRD reveals the formation of potassium bicarbonate and potassium metavanadate species (Figs. 4c, d, S6, and Table S2).

Discussion

The direct observation of the spectral signature of interfacial CO_2 is highly unexpected and opens new avenues to investigate CO_2 reactivity at liquid interfaces. The fact that the υ_3 asymmetric stretch of CO_2 is SFG active (both IR and Raman active) at the orthovanadate solution interface provides key insights into the interfacial interactions. In the gas phase, this mode is only IR active with a frequency of 2,350 cm^{-1} (19). Our DFT calculations indicate that as the CO_2 molecule bends, due to its interactions with water and/or orthovanadate, the Raman activity of this mode increases, and its frequency begins to redshift. Previous studies suggested bent CO_2–oxoanion structures as intermediate during the transformation from CO_2 to carbonate (16, 18). Our DFT calculations further reveal that protonated orthovanadate, i.e. $[HVO_4]^{2-}$, can bend CO_2 molecules to an O–C–O angle of 175°, sufficient for Raman activity (Fig. 1e). DFT calculations tend to overestimate the absolute value of the vibrational frequencies; however, the 10–15 cm^{-1} shift in the frequency is a more reliable parameter and similar to the experimental observation (see Fig. S7) (33). The experimental frequency of 2,336 cm^{-1} is also red-shifted compared with the hydrated CO_2 vibrational signature (19), suggesting that CO_2 adsorbed at the air/liquid interface is involved in relatively strong interactions, explaining its persistence under ambient atmosphere (inset of Fig. 1d). Ab initio molecular dynamics simulations, better

reflecting the complex interfacial environment, will be performed in the future.

A comparable direct observation of interfacial CO_2 was reported at a platinum electrode—ionic liquid interface during CO_2 reduction, where the CO_2 stretching frequency was at 2,348 cm^{-1} (21). It was suggested that CO_2 formed an intermediate species with the cation of the ionic liquid (1-ethyl-3-methylimidazolium), making it SFG active. Although our system differs, being at the air/water interface, and not electrochemically driven, with (bi)carbonate as its final product, this prior study provides supportive evidence to the possible formation of stable intermediate species detectable by SFG.

Orthovanadate hydrates CO_2 more strongly than molybdate due to its differentiating properties. HVO_4^{2-} is the most dominant and reactive vanadium (V) species under all solution conditions of pH and vanadium concentration (Fig. S9a and b), whereas our speciation calculations show that MoO_4^{2-} is the most dominant molybdate species under our solution conditions ([Molybdate] = 100 mM–2.0 M, and pH = 9.0–12.0; Fig. S9c and d). HVO_4^{2-} has a basic –OH group that directly binds to CO_2 (Fig. 1c). The presence of this hydroxyl group in addition to the two negative charges localized on two oxygen atoms contribute to the high catalytic activity of orthovanadate in hydrating CO_2 (see mechanism in Fig. 3b) (34, 35). Furthermore, for an inorganic oxyanion to accelerate CO_2 absorption, it must have a high pK_a value (17). The active V (V) species in CO_2 hydration, HVO_4^{2-} and $HV_2O_7^{3-}$ have pK_a values of 13.4 and 9.74, respectively (36). Therefore, HVO_4^{2-} and $HV_2O_7^{3}$ have very high catalytic activity for CO_2 hydration.

What are the implications of enhanced interfacial CO_2 concentration, and why was it not observed in other systems? It is possible that in commonly studied amine systems, the intermediate CO_2 capture products are mainly carbamates (11, 14), or the (bi)carbonate products are not surface/interface active or simply not SFG active. The bending of the CO_2 molecule from its linear geometry requires an asymmetric interaction with the orthovanadate. Nevertheless, recent SFG studies with amine systems suggest that increasing the residence time of CO_2 at the interface is beneficial for DAC, as it enhances the likelihood of reactive transport of CO_2 and binding as (bi)carbonate species (6, 14, 37). Indeed, the comparison of orthomolybdate and orthovanadate supports this view; orthomolybdate solutions show neither interfacial CO_2 nor carbonate products in the bulk following prolonged exposure. Finally, we note that this is a brief report of the direct observation of hydrated CO_2 at the air/liquid interface, but further investigations are needed to gain a deeper molecular insight into interfacial CO_2 hydration and adsorption at environmentally relevant interfaces.

The observation of interfacial (bi)carbonate species after longer exposure times and at higher orthovanadate concentrations (1–2 M) supports the hypothesis that interfacial CO_2 enhancement correlates with reactive transport of CO_2 into the bulk. Although numerous studies in the last two decades have utilized SFG spectroscopy on bulk carbonate and bicarbonate solutions, none reported direct spectral signatures of bicarbonate species at aqueous interfaces (7, 13, 27). Only organic carbonates, such as propylene carbonate, were observed at the liquid/air interface with a spectral signature around 1,750 cm^{-1} (38, 39). It is likely that the (bi)carbonate species observed in this study are visible to SFG due to their formation from highly ordered CO_2–orthovanadate complexes at the interface, resulting in orientational ordering. The dominant 1,412 and 1,640 cm^{-1} peaks with orthovanadate correspond to bidentate chelating bicarbonate symmetric and asymmetric stretches, which structurally resembles the intermediate orthovanadate–CO_2 observed in earlier stages. The mechanism of bidentate bicarbonate formation upon prolonged reaction of orthovanadate with CO_2 involves CO_2 binding to the basic –OH group of the HVO_4^{2-} species in a carbonic anhydrase intermediate mechanism (34), eventually dissociating into bicarbonate and metavanadate species (Fig. 3b).

We observe an increase in the intensity of the 1,412 cm^{-1} SFG signal with higher orthovanadate concentrations (Fig. 3a). Concurrently, bulk IR bicarbonate peaks also increase in intensity (Fig. 4a). This suggests that the surface species are relatively stable and are also transported into the bulk, creating ideal conditions for DAC. Conversely, with orthomolybdate solutions, (bi)carbonate species are observed only at 2 M concentration, with multiple peaks in the SFG spectra indicating more heterogeneous orientational ordering (Fig. 3c and Table S1). These (bi)carbonate products are limited to the interface with no significant presence in the bulk (Fig. 4b). A similar observation was made with $[Nb_6O_{19}]^{8-}$ solutions in our recent study. In that case, the solutions with K, Rb, and Cs counter ions showed mainly 1,412 cm^{-1} peak at the surface and a significant amount of carbon capture products in the bulk. However, solutions with tetramethylammonium (TMA) cation showed multiple SFG (bi)carbonate features but no significant carbon capture in the bulk. In that case, we attributed the lack of interface to bulk transport to the hydrophobic, and hence, surface-active nature of TMA. In the molybdate case, the reason may be the lower charge of molybdate (2– vs. 3– for orthovanadate) or a few number of free oxo-ligands (2 vs. 3 for orthovanadate), and hence increased hydrophobicity.

Before concluding, we rule out the possibility that the observed CO_2 signal is an artifact of the SFG setup. Given that the IR power is strongly absorbed by ambient CO_2, one might argue that the region between R and P branches appears as a peak. However, if this were the case, then the peak should be positioned at 2,350 cm^{-1}, precisely between the R and P branches (19). Furthermore, if the peak were an artifact of the laser setup, it would appear under all solution conditions. Nonetheless, as demonstrated, the peak responds specifically to the solution and reaction conditions and only appears at the surface of orthovanadate solutions. Moreover, the peak persists even after removing the CO_2-enhanced atmosphere (Fig. 1d), indicating that it is not affected by the bulk atmosphere above the surface and is indeed a genuine surface signal. All control experiments and additional details are provided in the Supplementary material.

Conclusion

In this study, we have reported the first direct observation of hydrated CO_2 and subsequent (bi)carbonate product formation at the air/water interface using SFG spectroscopy. The increased interfacial CO_2 concentration is advantageous for enhanced reactive capture of CO_2. However, if the products are not effectively transported into the bulk, they may obstruct the interface and hinder the process. As our focus was on the direct observation of interfacial products, we worked with smooth, stable air/liquid interfaces. It is reasonable to consider that under more realistic conditions, with agitation and stirring of the liquid, some of these effects might differ. Additionally, it is possible to control the interface with surfactants as proposed in earlier studies (40, 41). The direct observation of CO_2 and captured carbonates facilitates a rational comparison and contrast of these effects. We believe that this work will pave new paths in interfacial investigations. Lastly, this research contributes another example to the potential uses of oxoanions in CO_2 extraction (15, 42–44).

Materials and methods

SFG spectrometer

SFG experiments were conducted with an EKSPLA spectrometer, which has been described in the earlier publications (45, 46). Briefly, 1,064 nm laser pulse from a mode-locked Nd:YAG laser (EKSPLA, 29 ps, 50 Hz) is split, and frequency is doubled to 532 nm inside a harmonic unit. One of the 532 nm beams is directly used to probe the sample while the remaining beams are parametrically combined to generate a tunable IR beam. The beams are overlapped on the air/water interface in space and time in a reflection geometry; the visible and IR excitation angles, with respect to the sample normal, are $\theta_{vis} = 60°$ and $\theta_{IR} = 55°$, respectively. The 532 nm polarization is adjusted with a $\lambda/2$ waveplate, and the SFG signal is selected using a Glan polarizer. SFG spectra were collected at the air/liquid interface of aqueous solutions. After the sample, the SFG signal is directed to a monochromator and collected with a photomultiplier tube (Hamamatsu, R7899). Each spectrum was collected with a 4-cm^{-1} increment over the ranges 1,200–1,800, 2,200–2,400, and 3,000–3,800 cm^{-1} average of 50 laser shots per point. SFG spectra were collected in *ssp* polarization combination (s-SFG, s-VIS, and *p*-IR) and normalized to gold under the same experimental conditions.

SFG measurements at the air/liquid interface of CO_2 capture experiments

SFG spectra were collected at the air/liquid interface of aqueous solutions in a 1.0-inch diameter polytetrafluoroethylene (PTFE) dish. The PTFE dish was placed in a sealed homemade chamber designed specifically for the SFG measurements with two KBr windows for the input and output laser beams. Short-time SFG measurements were conducted in the sample cell during the exposure of the liquid samples to CO_2 dry ice. For prolonged exposure experiments, aqueous solutions were placed in the same PTFE dish and exposed to a CO_2-rich environment in a vacuum desiccator (~3–4 lbs dry ice) for ~15 h; then SFG spectra were collected on the samples before and after reaction with CO_2. Control measurements with varying pH and solution conditions are provided in Figs. S1–S4.

Bulk and solid characterization of CO_2 capture products

Attenuated total reflectance (ATR)-FTIR data were collected with a Nicolet Nexus 870 FTIR spectrometer with an ATR accessory with the same aqueous solutions used for SFG measurements. PXRD for all structures was collected on the solid products of CO_2 capture experiments at 150 K, on a Rigaku Oxford Diffraction Synergy-S equipped with a PhotonJet-S Cu source ($\lambda = 1.54178$ Å) or Mo source ($\lambda = 0.71073$) and a HyPix-6000HE photon counting detector. TGA was performed on TA Instruments SDT Q600, and MS was collected by Hiden Gas Analyzer HPR-20 QIC EGA. About 10 mg of the sample was transferred into alumina crucibles for measurements under Argon gas flow (the purge flow is 100 mL/min) up to 900 °C at the heating rate of 10 °C per minute. Approximately 90 min of Ar gas chamber flush (100 mL/min) was operated before the TGA–MS experiment to minimize the background noise.

Computational methods

Density functional theory calculations were carried out in the Gaussian 16 Rev. A.03 software package (47) with the CAM-B3LYP functional (48) and the default ultrafine integration grid. Carbon, oxygen, and hydrogen were modeled with the 6-31 +G* basis set, while LANL2DZ (49) was used for vanadium. The isolated CO_2 calculations for the bond angle scan were performed in vacuo without empirical dispersion. The $[HVO_4]^{2-}$–CO_2 system was embedded in an implicit water solvation environment through the polarizable continuum model (50). To more accurately account for the weak, noncovalent interaction between $[HVO_4]^{2-}$ and CO_2, the GD3 empirical dispersion correction (51) was included.

Acknowledgments

The authors thank Thomas Persinger for the SFG sample cell design. Part of this work was conducted at ANL, operated by UChicago Argonne, LLC for the United States Department of Energy.

Supplementary Material

Supplementary material is available at *PNAS Nexus* online.

Funding

This work was supported by the US Department of Energy, Basic Energy Sciences, grant DE-SC0022278.

Author Contributions

M.R.: conceptualization, data curation, investigation, methodology, writing—original draft, review, and editing. Z.M.: investigation, writing—review and editing. J.S.H.: formal analysis, investigation, writing—review and editing. T.J.Z.: supervision, funding acquisition. M.N.: conceptualization, supervision, funding acquisition, writing—review and editing. A.U.: conceptualization, supervision, funding acquisition, methodology, writing—review and editing.

Data Availability

All Cartesian structures and input files have been deposited on this public GitHub repository: https://github.com/tjz21/CO2_SFG_DFT. All experimental data are included in the manuscript and Supplementary material.

References

1 Wu X, Krishnamoorti R, Bollini P. 2022. Technological options for direct air capture: a comparative process engineering review. *Annu Rev Chem Biomol Eng*. 13:279–300.
2 Sanz-Pérez ES, Murdock CR, Didas SA, Jones CW. 2016. Direct capture of CO_2 from ambient air. *Chem Rev*. 116:11840–11876.
3 McQueen N, *et al*. 2021. A review of direct air capture (DAC): scaling up commercial technologies and innovating for the future. *Prog Energy*. 3:032001.
4 Chowdhury S, Kumar Y, Shrivastava S, Patel SK, Sangwai JS. 2023. A review on the recent scientific and commercial progress on the direct air capture technology to manage atmospheric CO_2 concentrations and future perspectives. *Energy Fuels*. 37: 10733–10757.
5 Uysal A. 2023. Aqueous interfaces in chemical separations. *Langmuir*. 39:17570–17580.
6 Kumar N, *et al*. 2024. Adsorption, orientation, and speciation of amino acids at air–aqueous interfaces for the direct air capture of CO_2. *Langmuir*. 40:14311–14320.

7 Hua W, Chen X, Allen HC. 2011. Phase-sensitive sum frequency revealing accommodation of bicarbonate ions, and charge separation of sodium and carbonate ions within the air/water interface. *J Phys Chem A*. 115:6233–6238.

8 Lam RK, *et al.* 2017. Reversed interfacial fractionation of carbonate and bicarbonate evidenced by X-ray photoemission spectroscopy. *J Chem Phys*. 146:094703.

9 Devlin SW, *et al.* 2023. Agglomeration drives the reversed fractionation of aqueous carbonate and bicarbonate at the air–water interface. *J Am Chem Soc.* 145:22384–22393.

10 Abe H, Takeshita A, Sudo H, Akiyama K. 2020. CO_2 capture and surface structures of ionic liquid-propanol solutions. *J Mol Liq*. 301:112445.

11 McWilliams LE, Valley NA, Vincent NM, Richmond GL. 2017. Interfacial insights into a carbon capture system: CO_2 uptake to an aqueous monoethanolamine surface. *J Phys Chem A*. 121: 7956–7967.

12 McWilliams LE, Valley NA, Wren SN, Richmond GL. 2015. A means to an interface: investigating monoethanolamine behavior at an aqueous surface. *Phys Chem Chem Phys*. 17:21458–21469.

13 Tarbuck TL, Richmond GL. 2006. Adsorption and reaction of CO_2 and SO_2 at a water surface. *J Am Chem Soc.* 128:3256–3267.

14 Premadasa UI, *et al.* 2023. Chemical feedback in the self–assembly and function of air–liquid interfaces: insight into the bottlenecks of CO_2 direct air capture. *ACS Appl Mater Interfaces*. 15(15):19634–19645.

15 Mao Z, *et al.* 2024. Carbon dioxide capture by niobium polyoxometalate fragmentation. *J Am Chem Soc*. 146:19489–19498.

16 Phan DT, Maeder M, Burns RC, Puxty G. 2014. Catalysis of CO_2 absorption in aqueous solution by inorganic oxoanions and their application to post combustion capture. *Environ Sci Tech*. 48: 4623–4629.

17 Nicholas NJ, da Silva G, Kentish S, Stevens GW. 2014. Use of vanadium(V) oxide as a catalyst for CO_2 hydration in potassium carbonate systems. *Ind Eng Chem Res*. 53:3029–3039.

18 Phan DT, Maeder M, Burns RC, Puxty G. 2015. Catalysis of CO_2 absorption in aqueous solution by vanadate and sulfate and their application to post combustion capture. *Int J Greenhouse Gas Control*. 36:60–65.

19 Li J, Guo J, Dai H. 2022. Probing dissolved CO_2(aq) in aqueous solutions for CO_2 electroreduction and storage. *Sci Adv*. 8: eabo0399.

20 Spearrin RM, Ren W, Jeffries JB, Hanson RK. 2014. Multi-band infrared CO_2 absorption sensor for sensitive temperature and species measurements in high-temperature gases. *Appl Phys B*. 116: 855–865.

21 Rosen BA, *et al.* 2012. In situ spectroscopic examination of a low overpotential pathway for carbon dioxide conversion to carbon monoxide. *J Phys Chem C*. 116:15307–15312.

22 Collins SE, Baltanás MA, Bonivardi AL. 2006. Infrared spectroscopic study of the carbon dioxide adsorption on the surface of Ga_2O_3 polymorphs. *J Phys Chem B*. 110:5498–5507.

23 Wijnja H, Schulthess CP. 1999. ATR–FTIR and DRIFT spectroscopy of carbonate species at the aged γ-Al_2O_3/water interface. *Spectrochim Acta A Mol Biomol Spectrosc.* 55:861–872.

24 Sthoer A, *et al.* 2022. La^{3+} and Y^{3+} interactions with the carboxylic acid moiety at the liquid/vapor interface: identification of binding complexes, charge reversal, and detection limits. *J Colloid Interface Sci.* 608:2169–2180.

25 Musegades LJ, Curtin OP, Cyran JD. 2024. Determining the surface pK_a of perfluorooctanoic acid. *J Phys Chem C*. 128:1946–1951.

26 Köck E-M, Kogler M, Bielz T, Klötzer B, Penner S. 2013. In situ FT-IR spectroscopic study of CO_2 and CO adsorption on Y_2O_3, ZrO_2, and Yttria-stabilized ZrO_2. *J Phys Chem C*. 117:17666–17673.

27 Du H, Liu J, Ozdemir O, Nguyen AV, Miller JD. 2008. Molecular features of the air/carbonate solution interface. *J Colloid Interface Sci.* 318:271–277.

28 Bonn M, Nagata Y, Backus EHG. 2015. Molecular structure and dynamics of water at the water–air interface studied with surface-specific vibrational spectroscopy. *Angew Chem Int Ed*. 54:5560–5576.

29 Chiang K-Y, *et al.* 2022. The dielectric function profile across the water interface through surface-specific vibrational spectroscopy and simulations. *Proc Natl Acad Sci U S A*. 119:e2204156119.

30 Boily J-F, *et al.* 2019. Hydrogen bonding and molecular orientations across thin water films on sapphire. *J Colloid Interface Sci.* 555:810–817.

31 Guo Q, *et al.* 2023. A theoretical analysis of the vibrational modes of ammonium metavanadate. *RSC Adv*. 13:15975–15980.

32 Onodera S, Ikegami Y. 1980. Infrared and Raman spectra of ammonium, potassium, rubidium, and cesium metavanadates. *Inorg Chem*. 19:615–618.

33 Wong MW. 1996. Vibrational frequency prediction using density functional theory. *Chem Phys Lett*. 256:391–399.

34 Guo D, *et al.* 2011. Borate-catalyzed carbon dioxide hydration via the carbonic anhydrase mechanism. *Environ Sci Technol*. 45: 4802–4807.

35 Sharma MM, Danckwerts PV. 1963. Catalysis by Brönsted bases of the reaction between CO2 and water. *Trans Faraday Soc*. 59: 386–395.

36 Crans DC, Tracey AS. 1998. The chemistry of vanadium in aqueous and nonaqueous solution. In: Crans DC, Tracey AS, editors. *Vanadium compounds*. American Chemical Society, p. 2–29.

37 Premadasa UI, *et al.* 2024. Synergistic assembly of charged oligomers and amino acids at the air–water interface: an avenue toward surface-directed CO2 capture. *ACS Appl Mater Interfaces*. 16:12052–12061.

38 Wang L, Peng Q, Ye S, Morita A. 2016. Surface structure of organic carbonate liquids investigated by molecular dynamics simulation and sum frequency generation spectroscopy. *J Phys Chem C*. 120:15185–15197.

39 Peng Q, Liu H, Ye S. 2017. Adsorption of organic carbonate solvents on a carbon surface probed by sum frequency generation (SFG) vibrational spectroscopy. *J Electroanal Chem*. 800:134–143.

40 Kumal RR, Wimalasiri PN, Servis MJ, Uysal A. 2022. Thiocyanate ions form antiparallel populations at the concentrated electrolyte/charged surfactant interface. *J Phys Chem Lett*. 13: 5081–5087.

41 Nayak S, Kumal RR, Uysal A. 2022. Spontaneous and ion-specific formation of inverted bilayers at air/aqueous interface. *Langmuir*. 38:5617–5625.

42 Ribó EG, *et al.* 2024. Implementing vanadium peroxides as direct air carbon capture materials. *Chem Sci*. 15:1700–1713.

43 Hirschi JS, Nyman M, Zuehlsdorff TJ. 2024. Electronic structure and CO_2 reactivity of group IV/V/VI tetraperoxometalates. *J Phys Chem A*. 128:7785–7794.

44 Arteaga A, *et al.* 2024. The role of alkalis in orchestrating uranyl-peroxide reactivity leading to direct air capture of carbon dioxide. *Chem Eur J*. 30:e202301687.

45 Rock W, Qiao B, Zhou T, Clark AE, Uysal A. 2018. Heavy anionic complex creates a unique water structure at a soft charged interface. *J Phys Chem C*. 122:29228–29236.

46 Nayak S, Kumal RR, Lee SE, Uysal A. 2023. Elucidating trivalent ion adsorption at floating carboxylic acid monolayers: charge reversal or water reorganization? *J Phys Chem Lett*. 14: 3685–3690.
47 Frisch MJ, *et al*. 2016. *Gaussian 16, Revision A.03*. Wallingford (CT): Gaussian Inc.
48 Yanai T, Tew DP, Handy NC. 2004. A new hybrid exchange–correlation functional using the Coulomb-attenuating method (CAM-B3LYP). *Chem Phys Lett*. 393:51–57.
49 Hay PJ, Wadt WR. 1985. Ab initio effective core potentials for molecular calculations. Potentials for the transition metal atoms Sc to Hg. *J Chem Phys*. 82:270–283.
50 Tomasi J, Mennucci B, Cammi R. 2005. Quantum mechanical continuum solvation models. *Chem Rev*. 105:2999–3094.
51 Grimme S, Antony J, Ehrlich S, Krieg H. 2010. A consistent and accurate ab initio parametrization of density functional dispersion correction (DFT-D) for the 94 elements H-Pu. *J Chem Phys*. 132: 154104.